Available online at www.sciencedirect.com
SCIENCE DIRECT
ELSEVIER
Journal of the European Ceramic Society 26 (2006) 1121–1130
ECERS
www.elsevier.com/locate/jeurceramsoc

Size and shape characterization of polydisperse short-fiber systems

Willi Pabst [a,*], Christoph Berthold [b], Eva Gregorová [a]

[a] *Department of Glass and Ceramics, Institute of Chemical Technology Prague, Technická 5, 166 28 Prague 6, Czech Republic*
[b] *Institut für Geowissenschaften, Arbeitsbereich Mineralogie und Geodynamik (Angewandte Mineralogie), Universität Tübingen, Wilhelmstrasse 56, 72074 Tübingen, Germany*

Received 30 June 2004; received in revised form 12 January 2005; accepted 23 January 2005
Available online 8 March 2005

Abstract

Two wollastonites, polydisperse with respect to size and shape, are characterized by image analysis. Aspect ratios are calculated for individual particles (1000–1500 objects) from the minimum and maximum Feret diameters measured. Although scatter is large (approximately 50%), average aspect ratios are well reproducible and approximately size-invariant, approximately 5 and 16 for wollastonite WM 45 and HSV 45, respectively. A transformation procedure is proposed and applied to transform the number-weighted size distributions obtained via image analysis into volume-weighted size distributions that can be compared with laser diffraction. The laser diffraction medians (21.6 μm and 29.1 μm for WM 45 and HSV 45, respectively) are close to the medians of the minimum Feret diameter distributions (20.6 μm and 29.9 μm for WM 45 and HSV 45, respectively). This is clear evidence of the fact that laser diffraction results need not at all correspond to projected area diameters determined by image analysis.

Keywords: Fibers; Whiskers; Optical microscopy; Electron microscopy; Image analysis; Wollastonite

1. Introduction

The measurement of particle size distributions is a standard operation for the characterization of ceramic raw materials, natural or synthetic. Among the most important methods for particle size analysis in the supermicron range today are sedimentation methods and laser diffraction methods, while sieving has lost its significance as an analytical tool, although it is still used by raw material producers for particle size classification. The reader can refer to a number of excellent references, textbooks as well as monographs and review articles, to get an overview on current methods and equipment, e.g. Refs.[1–5]. In contrast to the methods just mentioned, which can be termed ensemble methods, because size distributions are obtained without reference to size information for single objects, counting methods infer size distributions by evaluating a large number of single measurements. Examples of counting methods are electrozone sensing (Coulter counter principle), SPOS (single-particle optical sensing) and, most important of all, microscopic image analysis. Of these, only image analysis yields unbiased size information without a priori assumptions on particle shape. All other methods of particle size analysis assume, not only for reasons of convenience but mainly owing to the lack of a better alternative, spherical particle shape. Therefore, size is expressed in terms of equivalent diameters, i.e. diameters of hypothetical spheres (homogeneous and isotropic) which have a certain geometric characteristic (e.g. volume, surface), behavior (e.g. settling velocity) or property (e.g. the capability to evoke a certain disturbance in an electrical or electromagnetical field) in common with the particle in question. The fact that usually only equivalent diameters are measured implies that only for spherical particles (and approximately for non-spherical but isometric ones) coincidence of particle size measurements can be expected. In the case of anisometric particles, e.g. elongated or flaky ones (say fibers/whiskers or platelets) the result of the size measurement depends on the size measure chosen, i.e. the method applied, because the physical measuring principles are different and the mathematical evaluation algo-

* Corresponding author.
E-mail address: pabstw@vscht.cz (W. Pabst).

0955-2219/$ – see front matter © 2005 Elsevier Ltd. All rights reserved.
doi:10.1016/j.jeurceramsoc.2005.01.053

rithms assume spherical shape all the way. Indeed, "particle size" is not even uniquely defined for anisometric particles.

For flaky particles (platelets) it has been shown that the difference between sedimentation and laser diffraction results can be exploited to quantify shape information to a certain degree.[6–10] However, this approach cannot be used for elongated particles (fibers). Moreover, depending on the hydrodynamical situation, orientation effects of fibers in the flow-through cells of laser instruments can lead to strongly non-circular diffraction patterns, which can have a strong impact on the result when the photodetector is not equivalent to a full circle.[11] Therefore, in this case microscopic image analysis is an indispensible tool to obtain unbiased information on the size and morphology of fiber systems. Indeed, it seems that, in spite of all disadvantages and difficulties, image analysis is so far the most reliable source of unbiased information on particle size and shape in the case of fibers. At the moment at least, where new combined size- and shape-characterization equipment is beginning to conquer the market, image analysis represents the best method with the capability to provide benchmark results.

Therefore, it is the aim of the present paper to show, taking two types of wollastonite as paradigmatic examples, how polydisperse short-fiber systems can be characterized by microscopic image analysis with respect to size and shape. From the measured minimum and maximum Feret diameters aspect ratios are calculated for each individual particle. Arithmetic means of the aspect ratios are calculated for the individual size classes, together with the corresponding standard deviations. The latter serve to assess the representativity of the mean values and to test the size-dependence of the mean aspect ratios. A transformation procedure is proposed and applied to transform the number-weighted size distributions obtained via image analysis into volume-weighted size distributions in order to enable a comparison with size distributions measured by laser diffraction.

2. Shape and size measures for short fibers

Isometric particles have approximately the same size in all directions. Apart from the ideal case of spheres, isometric are e.g. all regular polyhedra (tetrahedra, cubes, octahedra, dodecahedra and icosahedra) and many other facetted and irregular particles. Anisometric particles have at least one distinguished direction along which their size is significantly larger or smaller than perpendicular to it. The simplest model shapes for approximating real anisometric particles are rotational ellipsoids (i.e. prolate and oblate spheroids) and circular cylinders (i.e. rods and discs or fibers and platelets). In both cases shape can be quantified via a single number, the aspect ratio. It is evident that the first is the more natural from a principal point of view, because it includes the sphere as a special case. Moreover, it is only for spheroids that the hydrodynamic problem of particle motion in a viscous fluid can be solved exactly. This is the reason why spheroids are the preferred model shapes e.g. in the rheology of fiber and platelet suspensions.[12–17] Defining the aspect ratio R as the ratio between the length of the rotational axis and the extension perpendicular to it (height-diameter ratio in the case of cylinders) one can distinguish prolate (elongated) particles with $R > 1$ and oblate (flaky) particles with $R < 1$.

Of course, for real particle systems (powders), which are usually polydisperse with respect to size and shape, the determination of "the" aspect ratio is not an easy task and need not even be useful in all cases, since shape (quantified via the aspect ratio) need not be (and in general is not) size-invariant. In other words, similar to the size, also the shape (aspect ratio) exhibits a distribution. In the case of oblate particles (discs) certain shape information, related to the aspect ratio, can be extracted from the comparison of sedimentation and laser diffraction data,[6–10] but the interpretation of these results is principally complicated by the fact that, in addition to the size distribution, there is a superimposed shape distribution in a real particle system. Nevertheless, in certain cases (viz., when the shape distribution is not correlated to the size distribution, i.e. for each size class the shape distribution is approximately the same), it can be useful to calculate an average aspect ratio $\overline{R}$ for the system as a whole. Such a unique "effective" value for the whole system (replacing de facto the broad aspect ratio distribution by a single Dirac distribution value) is for example necessary as an input information to apply effective viscosity formulae to real systems.[12–17] Unfortunately it is not a priori clear which kind of average should be taken in the case of a real polydisperse particle system. In the absence of a better alternative it seems reasonable to define the average aspect ratio $\overline{R}$ as the arithmetic mean of the measured individual aspect ratios.

Concerning size determination by microscopic image analysis, the projected area diameter (D_P) is often invoked as a size measure. It is the (2D equivalent) diameter of a circle whose area equals the area of the projected particle outline. In fact, it appears to be the most obvious "average size" measure for 2D objects. Anisometric particles, however, in particular those of strongly elongated shape, should be characterized by two numbers at least. A useful choice is the minimum and maximum Feret diameter,[1,4] i.e. the minimum extension of a (convex hull of a) particle outline and the extension in the perpendicular direction. This corresponds de facto to replacing the irregular particles (assumed to be in a stable position on the microscopic glass slide) by rotationally symmetric model shapes in 3D (e.g. prolate spheroids or cylindrical rods). Thus, in 2D the (convex hulls of the) particle outlines can be approximately replaced by ellipses or rectangles. The particle aspect ratio R can be expressed as the ratio between the maximum Feret diameter D_{max} and the minimum Feret diameter D_{min},

$$R = \frac{D_{max}}{D_{min}}. \quad (1)$$

In the case of an ellipse the minimum Feret diameter corresponds to the short axis, the maximum Feret diameter to

the long axis. In the case of a rectangle the meaning of the Feret diameters is trivial. Evidently, for fibers in 3D the minimum Feret diameter D_{min} is simply the fiber diameter D, the maximum Feret diameter D_{max} the fiber length L and the aspect ratio can be written as $R = L/D$. For more detailed information on image analysis and the definition of appropriate size measures the reader may consult the references[1,4,5,18]. When the minimum and maximum Feret diameter is measured for a selected particle, an approximate value of the projected area diameter D_P can be calculated (via the area of the ellipse or rectangle) without performing an explicit numerical evaluation of the pixels contained in the (possibly locally non-convex) projected particle outline. The projected area diameter calculated from the ellipse is

$$D_P^{ell} = \sqrt{D_{min} D_{max}}, \tag{2}$$

while that calculated from the rectangle is

$$D_P^{rect} = \sqrt{\frac{4 D_{min} D_{max}}{\pi}}. \tag{3}$$

Obviously $D_P \approx D_P^{rect} > D_P^{ell}$, i.e. for fibers the projected area diameters calculated from the rectangles D_P^{rect} are slightly larger than those calculated from ellipses D_P^{ell} and can usually be assumed to be closer to reality, i.e. closer to the projected area diameter D_P, which would be obtained by performing a numerical evaluation of pixels.

Apart from being more time-consuming and operator-dependent than other methods of particle size analysis, one major difficulty remains with image analysis: the primary results (size distributions) are number-weighted. That means that a direct comparison of results from image analysis with those from other methods yielding volume-weighted size distributions, e.g. laser diffraction, is not possible. In order to compare image analysis and laser diffraction results it is necessary to transform the image analysis results (so-called "q_0" frequency histograms/curves or "Q_0" cumulative histograms/curves) into volume-weighted distributions ("q_3" or "Q_3" histograms/curves). For real systems with anisometric particles this involves a tedious multi-step procedure. However, in cases where the shape is approximately size-invariant (i.e. where the same average value of the aspect ratio can be used for all size classes) this "$q_0 \rightarrow Q_3$ transformation" can be greatly simplified.

3. Construction of volume-weighted cumulative curves from image analysis data

Results obtained from image analysis cannot be directly compared with results obtained by other methods, e.g. laser diffraction. In order to compare the size distributions obtained by image analysis (primary data in the form of number-weighted frequency histograms, denoted q_0) with those obtained from laser diffraction (computer output in the form of volume-weighted cumulative curves, denoted Q_3), a transformation is necessary, termed here "$q_0 \rightarrow Q_3$ transformation". Let us explain the individual steps of this transformation procedure with the data set given in Table 1. The second column of Table 1 lists absolute frequencies, i.e. the number of objects whose projected area diameter comes to lie in a certain size class of width 3 μm around the mean value of the projected area diameter (mean value of the size class, given in the first column of Table 1), cf. Fig. 1. Obviously the few singular objects counted in the large-size region >85.5 μm are solely due to statistical scatter ("noise"). Due to their large size D_P these few objects will have an extremely large volume (scaling with D_P^3) and, can therefore, have a considerable influence on the volume-weighted size distribution, i.e. they would distort the whole cumulative curve. This scatter is a consequence of the finite (i.e. relatively small) number of objects counted. Although less obvious, a more detailed inspection shows that similar conclusions hold for all values in the region >58.5 μm, say. Of course, the exact value of this "cut-off size" D_C has to be fixed by inspection of each data set individually. The existence of D_C in polydisperse systems is justified on pragmatic grounds by the fact that multi-modal (more complex than bimodal) particle size distributions are in reality relatively rare and that the occurrence of single objects need not be statistically significant. Since this step implies a subjective decision of the operator it cannot be easily done automatically. As soon as the "cut-off size" is defined, the absolute frequencies in the size range $>D_C$ are re-ordered ("first re-ordering") by permutation from the highest to the lowest, i.e. in decreasing order. Since in this step all zero values between positive frequencies are artificially shifted to the end, the re-ordered frequency histogram as a whole ends at smaller sizes than the original one ("artificial damping"), cf. the third column in Table 1 and Fig. 2.

In order to transform the re-ordered q_0 frequency histogram (number-weighted) into a volume-weighted q_3 histogram (relative partial volumes of the respective size classes, with the volume of the whole system normalized to unity) one should in principle use the aspect ratio measured for each individual particle. Of course, as mentioned above, this tedious procedure is greatly simplified when the aspect ratio is assumed to be size-invariant: in this case the q_3 values simply scale with D_P^3, irrespective of the particular shape. The fourth column of Table 1 and Fig. 3 show the relative partial volumes of the respective size classes under such an assumption. There are peaks (so-called "modes") in the q_3 histogram (here at 64.5 μm, 79.5 μm and 97.5 μm) which are again obviously a consequence of the finite data set (i.e. the too small number of objects counted). Similar to the step before, a "second re-ordering" can be performed for all relative partial volumes in the size range $>D_C$ (here >58.5 μm), cf. Fig. 4 and the fifth column in Table 1. After all these steps it is a trivial task to finally sum up the relative volumes (corresponding to a numercial integration of the q_3 curve), cf. the sixth column in Table 1, and to draw a cumulative histogram or a smooth cumulative (Q_3) curve. Figs. 5 and 6 show the resulting Q_3

Table 1
Size distribution of wollastonite WM 45 in terms of projected area diameters; first column: projected area diameter D_P (mean value of the size class chosen), second and third column: absolute frequency (number of objects) q_0, fourth and fifth column: relative volume q_3, sixth column: cumulative volume Q_3

Projected area diameter (μm)	Absolute frequency (before first re-ordering)	Absolute frequency (after first re-ordering)	Relative volume (%) (before second re-ordering)	Relative volume (%) (after second re-ordering)	Cumulative volume (%)
10.5	15	15	0.04	0.04	0.0
13.5	112	112	0.63	0.63	0.7
16.5	197	197	2.02	2.02	2.7
19.5	197	197	3.33	3.33	6.0
22.5	189	189	4.91	4.91	10.9
25.5	151	151	5.71	5.71	16.7
28.5	108	108	5.71	5.71	22.4
31.5	76	76	5.42	5.42	27.8
34.5	48	48	4.50	4.50	32.3
37.5	42	42	5.06	5.06	37.3
40.5	41	41	6.22	6.22	43.5
43.5	26	26	4.88	4.88	48.4
46.5	21	21	4.82	4.82	53.3
49.5	22	22	6.09	6.09	59.3
52.5	14	14	4.62	4.62	64.0
55.5	11	11	4.29	4.29	68.3
58.5	6	6	2.74	3.67	71.9
61.5	5	6	3.19	3.51	75.4
64.5	6	6	3.67	3.19	78.6
67.5	3	5	3.51	2.74	81.4
70.5	2	3	2.40	2.40	83.8
73.5	2	2	1.81	2.29	86.1
76.5	6	2	2.04	2.12	88.2
79.5	2	2	2.29	2.04	90.2
82.5	0	1	1.28	1.93	92.1
85.5	0	1	1.43	1.81	94.0
88.5	1	1	1.58	1.75	95.7
91.5	1	1	1.75	1.58	97.3
94.5	1	1	1.93	1.43	98.7
97.5	0	1	2.12	1.28	100.0
100.5	1	0	0.00	0.00	100.0
103.5	0	0	0.00	0.00	100.0
106.5	1	0	0.00	0.00	100.0
109.5	0	0	0.00	0.00	100.0
112.5	1	0	0.00	0.00	100.0
Total	1308		100		

curves with linear and logarithmic abscissa, respectively. For reasons of comparison, Figs. 7 and 8 show also the resulting cumulative curves based on the original values (without re-ordering) and the values after first re-ordering only (without second re-ordering), cf. the fourth column of Table 1. Interestingly, although by mere visual inspection (Figs. 3 and 4) the "second re-ordering" appears to be a more severe manipulation with the results, it can be seen (Figs. 7 and 8) that

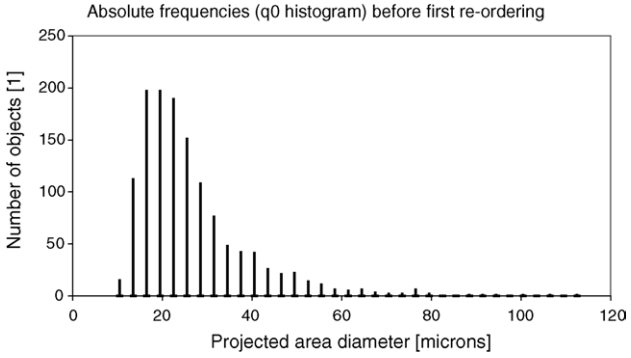

Fig. 1. Size distribution of wollastonite WM 45 in terms of projected area diameters; number-weighted frequency (q_0) histogram before first re-ordering.

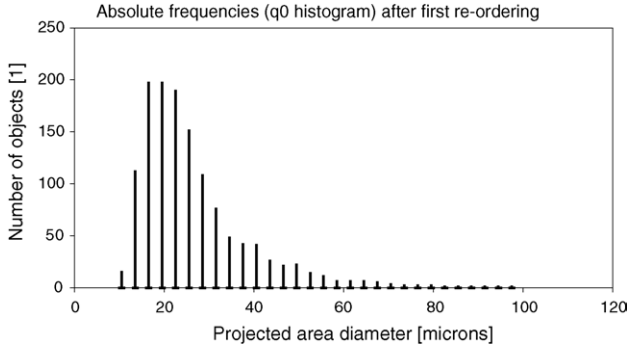

Fig. 2. Size distribution of wollastonite WM 45 in terms of projected area diameters; number-weighted frequency (q_0) histogram after first re-ordering.

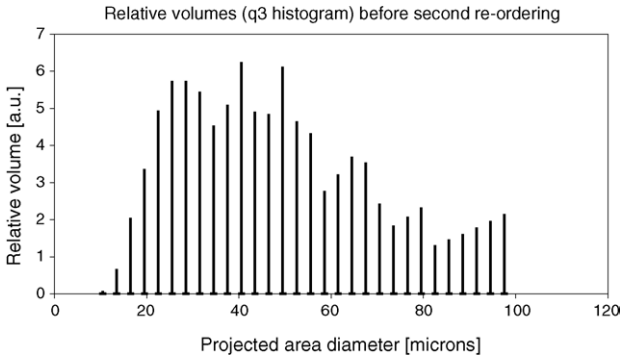

Fig. 3. Size distribution of wollastonite WM 45 in terms of projected area diameters; volume-weighted frequency (q_3) histogram before second re-ordering.

this is not the case and that, on the contrary, the "first re-ordering", although apparently less severe (Figs. 1 and 2) is the more decisive step. For approximate results, the second re-ordering step could be omitted, the first not. We emphasize that the necessity to chose a "cut-off size" D_C and to perform (at least first) "re-ordering" arises from the fact that the number of objects counted is finite (i.e. too small in practice). The more objects are counted, the larger D_C. No cut-off should be necessary in the asymptotic case of infinitely many objects. Summarizing, for usual data sets occurring in practice, the "$q_0 \rightarrow Q_3$ transformation" proposed consists of the following steps:

- Choosing a "cut-off size" D_C,
- "First re-ordering", corresponding to "artificial damping" (q_0 histogram),
- Calculation of relative volumes ($q_0 \rightarrow q_3$, possibly simplified by the assumption of a unique and size-invariant aspect ratio),
- "Second re-ordering" (q_3 histogram),
- Summing up the relative volumes ($q_3 \rightarrow Q_3$, "numerical integration").

Note that for data sets with an extremely large number of objects only the two steps $q_0 \rightarrow q_3$ and $q_3 \rightarrow Q_3$ are necessary.

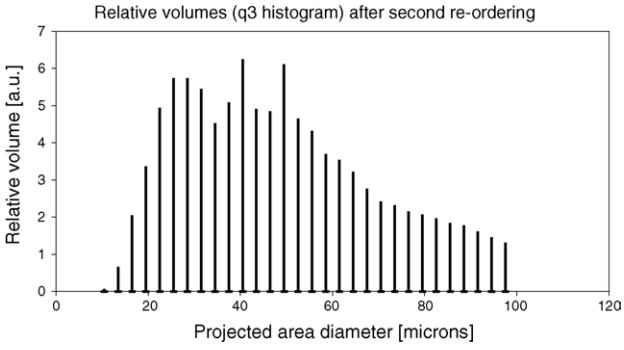

Fig. 4. Size distribution of wollastonite WM 45 in terms of projected area diameters; volume-weighted frequency (q_3) histogram after second re-ordering.

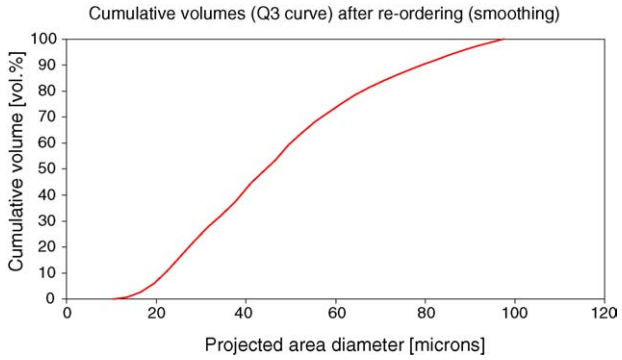

Fig. 5. Size distribution of wollastonite WM 45 in terms of projected area diameters; volume-weighted cumulative (Q_3) curve after re-ordering.

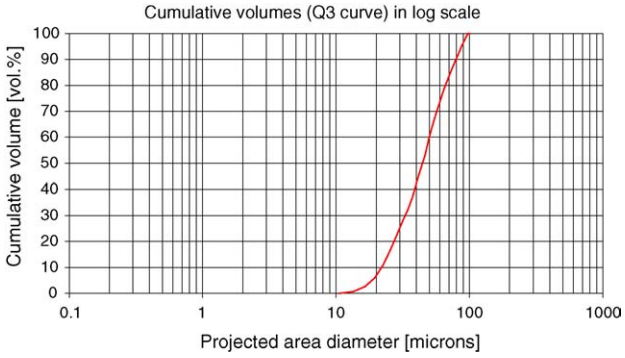

Fig. 6. Size distribution of wollastonite WM 45 in terms of projected area diameters; volume-weighted cumulative (Q_3) curve after re-ordering in log scale.

4. Experimental details

Two types of wollastonite ($CaSiO_3$) have been investigated: WM 45 (Franz Mandt GmbH, Wunsiedel/Germany) and HSV 45 (H. Osthoff-Petrasch GmbH, Norderstedt/Germany). According to the suppliers both types have a sieve size <45 μm. Figs. 9 and 10 show optical (Jenapol, Zeiss, Jena/Germany) and SEM (LEO Model 1450 VP, Electron Microscopy Ltd., Cambridge, UK) micrographs of types

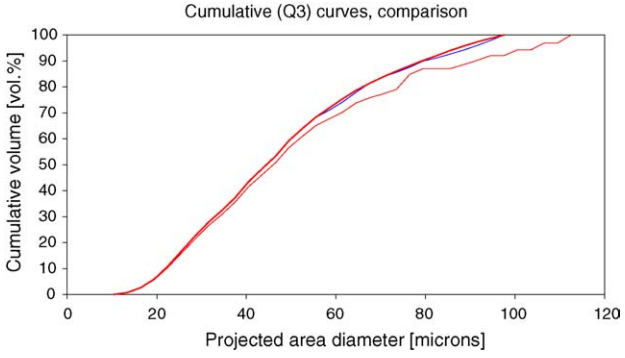

Fig. 7. Comparison of size distributions of wollastonite WM 45; final Q_3 curve after first and second re-ordering (bold full line) compared to the Q_3 curves without re-ordering (thin full line), and after first re-ordering only (thin dashed line).

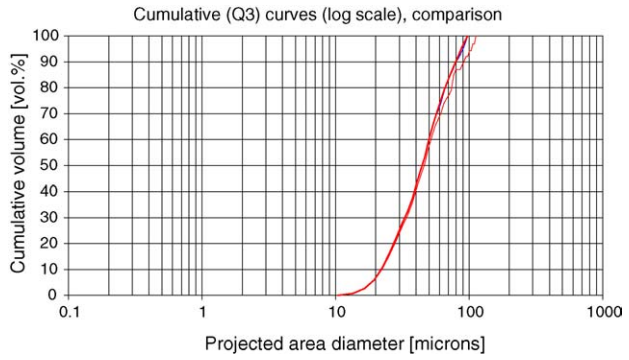

Fig. 8. Comparison of size distributions of wollastonite WM 45 in log scale (description see Fig. 6).

WM 45 and HSV 45, respectively. At first sight one may recognize that particles of WM 45 are on the average less elongated than particles of HSV 45. To quantify this statement image analysis was performed using a commercial image analysis software package (LUCIA G—version 4.81, Laboratory Imaging s.r.o., Prague/Czech Republic). For this purpose each particle that was visible in its full outline on the micrograph (24 and 13 micographs for WM 45 and HSV 45, respectively) was marked manually by circumscribing a rectangle. The total number of particles counted was 1308 and 1027 for WM 45 and HSV 45, respectively.[19] Length and width of the rectangle were considered as maximum and minimum Feret diameter D_{max} and D_{min} of the particle, respectively. D_{max} and D_{min} were used to calculate the particle aspect ratio R according to Eq. (1), while the area of the rectangle served to calculate the projected area diameter D_P according to Eq. (3). Additional investigations performed by other operators[20–22] are available that can be used to test the reproducibility and to assess the operator-dependence of the results. In Ref. 20 image analysis of the same micrographs has been performed with 1493 and 1003 counted objects for WM 45 and HSV 45, respectively. For type WM 45 the second operator used an inscribed five-point ellipse to mark the individual objects, type HSV 45 was marked by rectangles as in Ref. 19. Apart from microscopic image analysis, both types of wollastonite were measured (in dilute aqueous suspension) by laser diffraction using the particle sizer Analysette 22 (Fritsch GmbH, Idar-Oberstein/Germany).

5. Results and discussion

As a result of the internal structure (i.e. single-chain silicate structure) and preferred cleavage along the directions [1 0 0] and [0 0 1], the usual external shape of wollastonite particles, whether in their natural environment or after raw material processing, is that of irregular elongated needles (short fibers), cf. Figs. 9 and 10. In a first approximation, cylindrical rods can therefore be used as model shapes to model these particles.

Tables 2 and 3 list the arithmetic means, standard deviations and relative standard deviations of aspect ratios determined for wollastonites WM 45 and HSV 45, respectively, for each projected area diameter size class (arithmetic mean). The total averages calculated from the partial class averages are $\bar{R} = 4.9 \pm 1.2$ and $\bar{R} = 15.8 \pm 4.2$ for WM 45 and HSV 45, respectively. When the total average is calculated from the individual objects, the results are essentially the same, viz. $\bar{R} = 4.7$ and $\bar{R} = 16.2$ for WM 45 and HSV 45, respectively. The fact that the aspect ratio is not a unique value, even for a given size class, is reflected by the high relative standard

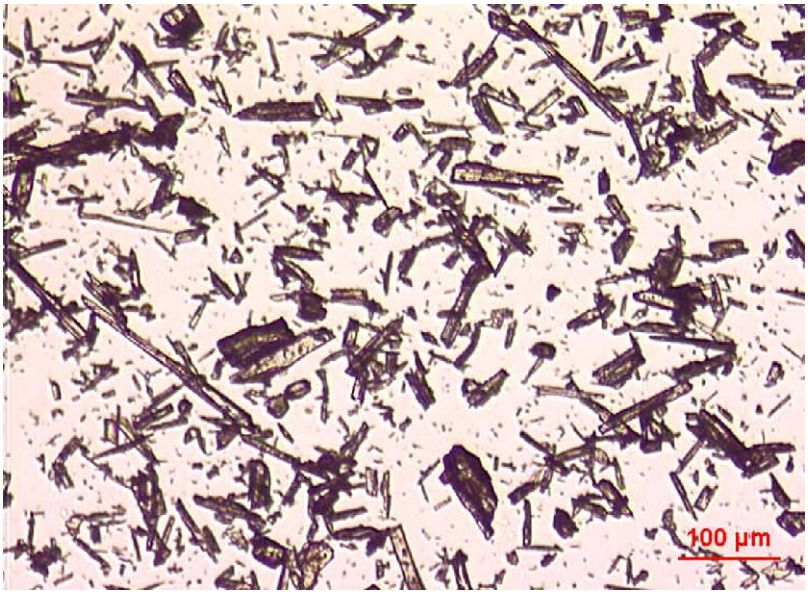

Fig. 9. Optical micrograph of wollastonite WM 45.

Fig. 10. SEM micrograph of wollastonite HSV 45.

Table 2
Aspect ratios (arithmetic means) for the various size classes of wollastonite WM 45

Projected area diameter (µm)	Aspect ratio *R* (arithmetic mean)	Absolute standard deviation	Relative standard deviation (%)
10.5	3.2	0.9	28.1
13.5	3.8	1.5	39.5
16.5	4.0	1.7	42.5
19.5	4.6	2.5	54.3
22.5	5.0	2.3	46.0
25.5	5.1	2.5	49.0
28.5	4.3	1.6	37.2
31.5	5.0	2.6	52.0
34.5	5.5	2.6	47.3
37.5	5.5	2.9	52.7
40.5	5.6	3.5	62.5
43.5	5.6	3.4	60.7
46.5	6.2	3.3	53.2
49.5	4.4	2.1	47.7
52.5	5.1	2.7	52.9
55.5	7.0	4.3	61.4
58.5	7.0	5.7	81.4
61.5	3.9	1.4	35.9
64.5	3.5	1.3	37.1
67.5	7.3	5.3	72.6
70.5	5.2	1.0	19.2
73.5	3.0	1.1	36.7
76.5	5.4	3.2	59.3
79.5	3.3	1.2	36.4
Total average from individual objects	4.7		
Total average from partial class averages	4.9		±49%

Table 3
Aspect ratios (arithmetic means) for the various size classes of wollastonite HSV 45

Projected area diameter (μm)	Aspect ratio R (arithmetic mean)	Absolute standard deviation	Relative standard deviation (%)
20.25	18.1	12.8	70.7
28.75	15.8	9.2	58.2
37.25	16.5	10.1	61.2
45.75	16.6	10.4	62.7
54.25	16.6	12.2	73.5
62.75	15.6	10.9	69.9
71.25	16.2	10.5	64.8
79.75	13.7	6.7	48.9
88.25	13.2	6.4	48.5
96.75	13.0	6.4	49.2
105.25	17.7	10.9	61.6
113.75	23.2	15.4	66.4
122.25	10.9	5.6	51.4
130.75	6.1	2.5	41.0
139.25	14.4	5.2	36.1
147.75	13.6	7.7	56.6
156.25	15.3	9.4	61.4
164.75	16.2	3.2	19.8
173.25	15.0	6.0	40.0
181.75	28.0	8.3	29.6
Total average from individual objects	16.2		
Total average from partial class averages	15.8		±54%

deviations (±49% and ±54% for WM 45 and HSV 45, respectively). This shows that for the materials investigated—as is true for most real polydisperse systems—the aspect ratio is not a precisely defined number but exhibits a relatively broad distribution, even within a selected size class. Another investigation of the same samples by a second operator[20] resulted in average aspect ratios of $\bar{R} = 4.4$ and $\bar{R} = 16.1$ and relative standard deviations of ±51% and ±55% for WM 45 and HSV 45, respectively, and in an earlier investigation a third operator[21,22] found an average aspect ratio of $\bar{R} = 4.75$ for WM 45. This excellent agreement increases our confidence in the reproducibility and reliability of the results. All findings clearly indicate that the average aspect ratio is significantly different for the two types of wollastonite. Although the aspect ratio is not given by a unique number, but by the average value (arithmetic mean) of a rather broad distribution (with a standard deviation of order 50%), there is no indication of any trend with size (the scatter of the mean values referring to the partial size classes is approximately 25%).

Figs. 11 through 14 show the volume-weighted size distributions (cumulative and frequency curves) of wollastonites WM 45 and HSV 45, respectively, as measured by laser diffraction. According to the results of laser diffraction, only 77 vol.% (WM 45) and 60 vol.% (HSV 45) are <45 μm, although according to the suppliers both types of wollastonite have a sieve size below 45 μm. The reason of this discrepancy is that laser diffraction measures a certain equivalent diameter, i.e. the diameter of a hypothetical sphere. Clearly, with growing degree of anisometry the differences between results obtained by different methods become more significant. The subsieve size (determined by

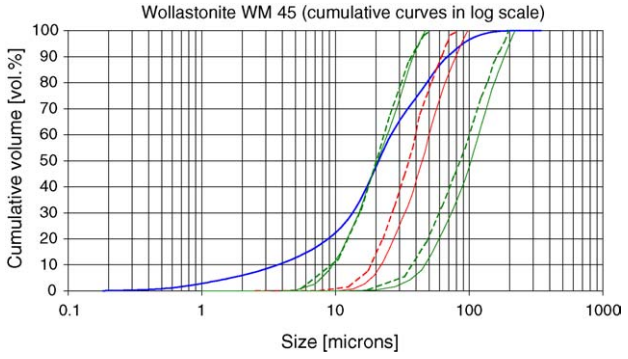

Fig. 11. Volume-weighted size distributions (cumulative curves Q_3) of wollastonite WM 45; bold line: laser diffraction size (LALLS equivalent diameter), thin lines (full, this work and Ref. 19 and dashed, second operator and Ref. 20): minimum Feret diameter (left), projected area diameter (center), maximum Feret diameter (right).

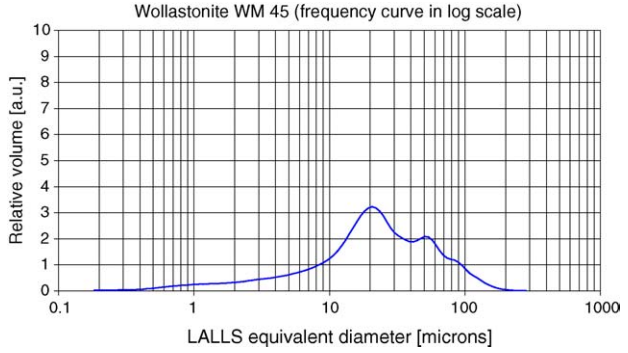

Fig. 12. Laser diffraction frequency curve q_3 of wollastonite WM 45.

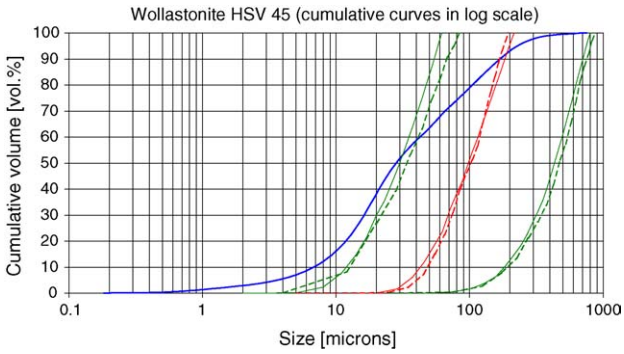

Fig. 13. Volume-weighted size distributions (cumulative curves Q_3) of wollastonite HSV 45; bold line: laser diffraction size (LALLS equivalent diameter), thin lines (full, this work and Ref. 19 and dashed, second operator and Ref. 20): minimum Feret diameter (left), projected area diameter (center), maximum Feret diameter (right).

the mesh size and shape of the sieve used for raw material classification) represents more or less the dimensions perpendicular to the length of the wollastonite needles.

In order to compare the results of image analysis and laser diffraction, the "$q_0 \rightarrow Q_3$ transformation" procedure described above has been applied to the image analysis data. In addition to the projected area diameters, the "$q_0 \rightarrow Q_3$ transformation" has been performed for maximum and minimum Feret diameters. The latter two results may cum grano salis be considered as representing the upper and lower bound, respectively, of all possible size distributions. Apart from the projected area diameter (a popular and convenient size measure), any other reasonable average size measure obtainable via image analysis, defined in whatever way, has to yield distributions that should lie between these bounds.

At first sight it is evident from Figs. 11 and 13 that the difference between the three transformed image analysis particle size distributions (PSDs) with respect to D_{min} (two curves on the left), D_P (two central curves) and D_{max} (two curves on the right) is more significant for the wollastonite with the higher aspect ratio (HSV 45). A more detailed inspection of the transformed image analysis PSDs reveals that there is rather satisfactory agreement between the measurements of the present paper (full lines) and earlier results obtained by the second operator (dashed lines), cf. Ref. 20. The slightly larger discrepancy of the results for D_P and D_{max} of WM 45 (Fig. 11) has to be assigned to the aforementioned fact that in this case inscribed five-point ellipses were used instead of circumscribed rectangles to mark the objects. This explains the smaller D_P values (smaller area of ellipse than of rectangle with the same aspect ratio) and the underestimated D_{max} values (due to irregularities at the fiber tip).

The laser diffraction PSDs are in both cases smaller than the PSDs in terms of D_P. For both types of wollastonite a considerable part of the laser diffraction PSD even violates the lower bound of image analysis results (PSD in terms of D_{min}) and the median size D_{50} of the laser diffraction PSDs (21.6 μm and 29.1 μm for WM 45 and HSV 45, respectively) is in both cases close to the median of the PSDs in terms of D_{min} (20.6 μm and 29.9 μm for WM 45 and HSV 45, respectively). This is clear evidence of the fact that laser diffraction results need not at all correspond to projected area diameters measured by image analysis for fibers lying in a stable position on a glass slide. The reason is that, due to the possible random orientation of the fibers in the flow-through cell of the laser diffractometer, the shortest fiber dimension can be largely over-represented in the laser diffraction results. Note, however, that the situation may change when preferential orientation (fiber alignment in flow direction) can be achieved during measurement, cf. Ref. 11. Above the median size the cumulative laser diffraction PSDs exhibit a "kink" (and the frequency curves a maximum, a so-called "mode"), which could be indicative of the fact that precisely this value (smallest-size mode of the laser diffraction frequency curve) corresponds to the thickness of the fibers. Evidently, the laser diffraction PSD is broader for the high-aspect ratio wollastonite HSV 45 than for the low-aspect ratio wollastonite WM 45. It can be conjectured, therefore, that in principle shape information should be contained in the structure of the laser diffraction frequency curves. Unfortunately, however, it is not possible to correlate the remainder of this structure of the laser diffraction frequency curves, e.g. the second mode at 50–60 μm for WM 45 (Fig. 12), the second mode at 40–80 μm and the broad plateau between 120 μm and 150 μm for HSV 45 (Fig. 14) with the shape information obtained from image analysis.

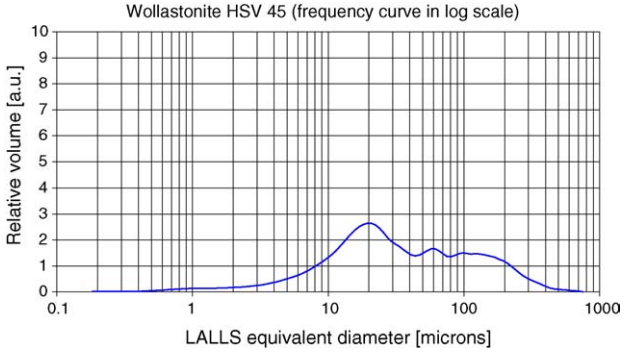

Fig. 14. Laser diffraction frequency curve q_3 of wollastonite HSV 45.

6. Conclusion and outlook

Two wollastonite systems, both polydisperse with respect to size and shape, have been characterized by microscopic image analysis. Aspect ratios have been calculated for each individual particle (1000–1500 objects) from the minimum and maximum Feret diameters measured. Although the scatter is large (relative standard deviation within a particular size class approximately 50%, relative scatter of the mean values among different size classes approximately 25%), the average aspect ratios are well reproducible and approximately size-invariant, approximately 5 for wollastonite WM 45 and

approximately 16 for wollastonite HSV 45. A transformation procedure ("$q_0 \rightarrow Q_3$ transformation") has been proposed and applied to transform the number-weighted size distributions obtained via image analysis into volume-weighted size distributions that can be compared with the results of laser diffraction.

The medians of the laser diffraction size distributions (21.6 μm and 29.1 μm for WM 45 and HSV 45, respectively) are in both cases close to the medians of the size distributions in terms of the minimum Feret diameter (20.6 μm and 29.9 μm for WM 45 and HSV 45, respectively). This is clear evidence of the fact that, in the case of fibers, laser diffraction results need not at all correspond to projected area diameters determined by image analysis.

The method proposed and applied in this work should be useful for size and shape characterization of all types of short-fiber systems. Although wollastonite fibers have been chosen here as a paradigmatic example, the key items of this paper, in particular the "$q_0 \rightarrow Q_3$ transformation" proposed, should be of general value for the characterization of fibers and whiskers used in ceramic and composite technology. The special results obtained (average aspect ratio and information about the size distribution) have been used as an input information in a recent investigation[23] on the influence of particle shape (and size) on suspension rheology (effective viscosity).

Acknowledgements

This work was part of the bilateral project "Size and shape characterization of particles in ceramic science and technology", supported by the Czech Ministry of Education, Youth and Sports (Grant no. CZE 01/012) and the German Bundesministerium für Forschung und Technik (BMFT) as well as the research program "Preparation and properties of advanced materials—modelling, characterization, technology", supported by the Czech Ministry of Education, Youth and Sports (Grant no. MSM 223100002). The support is gratefully acknowledged. Further we thank Dr. H. Schulz (Institut für Geowissenschaften, Universität Tübingen) for the SEM micrographs, our students S. Rosková, E. Kotulanová (ICT Prague) and C. Laforet (ENSCI Limoges and ICT Pague) for carefully operating the image analysis, as well as the Franz Mandt GmbH (Wunsiedel) and the H. Osthoff-Petrasch GmbH (Norderstedt) for providing free wollastonite samples.

References

1. Allen, T., *Particle Size Measurement* (*Vol 1, 5th ed.*). Chapman & Hall, London, 1997.
2. Bernhardt, C., *Particle Size Analysis: Classification and Sedimentation Methods*. Chapman & Hall, London, 1994.
3. Xu, R., *Particle Characterization: Light Scattering Methods*. Kluwer Academic Publishers, Dordrecht, 2000.
4. Scarlett, B., Characterization of particles and powders. In *Materials Science and Technology: Processing of Ceramics, Part I* (*Vol 17A*), ed. R. J. Brook. VCH, Weinheim, 1996, pp. 99–125.
5. Kaye, B. H., *Direct Characterization of Fine Particles*. John Wiley, New York, 1981.
6. Pabst, W., Kuneš, K., Havrda, J. and Gregorová, E., A note on particle size analysis of kaolins and clays. *J. Eur. Ceram. Soc.*, 2000, **20**, 1429–1437.
7. Pabst, W., Kuneš, K., Gregorová, E. and Havrda, J., Extraction of shape information from particle size measurements. *Br. Ceram. Trans.*, 2001, **100**, 106–109.
8. Pabst, W., Mikač, J., Gregorová, E. and Havrda, J., An estimate of orientation effects on the results of size distribution measurements for oblate particles. *Ceram.-Silikáty*, 2002, **46**, 41–48.
9. Lehmann, M., *Korngrössen- und Kornformcharakterisierung an Kaolinen, Ein Vergleich von Laserbeugungs- und Sedimentationsmethoden*. M.Sc. thesis, Universität Tübingen, 2003.
10. Lehmann, M., Berthold, C., Pabst, W., Gregorová, E. and Nickel, K. G., Particle size and shape characterization of kaolins—comparison of settling methods and laser diffraction. *Key Eng. Mater.*, 2004, **264–268**, 1387–1389.
11. Berthold, C., Klein, R., Lühmann, J. and Nickel, K. G., Characterization of fibres and fibre collectives with common laser diffractometers. *Part. Part. Syst. Charact.*, 2000, **17**, 113–116.
12. Brenner, H., Rheology of a dilute suspension of axisymmetric Brownian particles. *Int. J. Multiphase Flow*, 1974, **1**, 195–341.
13. Kitano, T., Kataoka, T. and Shirota, T., An empirical equation of the relative viscosity of polymer melts filled with various inorganic fillers. *Rheol. Acta*, 1981, **20**, 207–209.
14. Zirnsak, M. A., Hur, D. U. and Boger, D. V., Normal stresses in fibre suspensions. *J. Non-Newtonian Fluid Mech.*, 1994, **54**, 153–193.
15. Petrie, C. J. S., The rheology of fibre suspensions. *J. Non-Newtonian Fluid Mech.*, 1999, **87**, 367–402.
16. Petrich, M. P., Koch, D. L. and Cohen, C., An experimental determination of the stress-microstructure relationship in semi-concentrated fiber suspensions. *J. Non-Newtonian Fluid Mech.*, 2000, **95**, 101–133.
17. Pabst, W. and Gregorová, E., Rheology of platelet and fiber suspensions. In *Advances in Science and Technology: Proceedings of the 10th International Ceramics Congress CIMTEC 2002. Part A* (*Vol 30*), ed. P. Vincenzini. Techna, Faenza, 2003, pp. 609−616.
18. Russ, J. C. and Dehoff, R. T., *Practical Stereology* (*2nd ed.*). Kluwer Academic/Plenum Publishers, New York, 2000, pp. 45−109.
19. Laforet, C., *Microscopic Characterization of Anisometric Particles and Rheology of their Suspensions*. M.Sc. thesis, ENSCI Limoges/ICT, Prague, 2004.
20. Kotulanová, E., *Microscopic Characterization of Elongated Particles and their Suspension Rheology*. M.Sc. thesis, ICT, Prague, 2004 (in Czech).
21. Rosková, S., *Characterization of Anisometric Particles and Porous Materials*. M.Sc. thesis, ICT, Prague, 2003 (in Czech).
22. Rosková, S., Pabst, W. and Berthold, C., Size distribution measurement of short fibers by laser diffraction. In *Proceedings of the 5th Conference on Preparation of Ceramic Materials*, ed. B. Plešingerová and T. Kuffa. Technical University Košice, Košice, 2003, pp. 10–11 (in Czech).
23. Pabst, W., Gregorová, E. and Berthold, C., Particle shape and suspension rheology of short-fiber systems. *J. Eur. Ceram. Soc.*, 2006, **26**, 149–160.